Proceedings World Geothermal Congress 2020+1
Reykjavik, Iceland, April - October 2021

Source and Behavior of Stibnite Scaling: Case Study: Büyük Menderes Graben (Western Turkey)

[1]Serhat Tonkul, [2]Simona Regenspurg, [3]Mustafa M. Demir, [4]Alper Baba

[1,4]İzmir Institute of Technology, Department of Civil Engineering, Program of International Water Resources, 35430, Urla, İzmir, Turkey

[3]İzmir Institute of Technology, Department of Material Science and Engineering, 34530, Urla, İzmir, Turkey

[2]Helmholtz-Zentrum Potsdam, Deutsches GeoForschungsZentrum GFZ, Potsdam, Germany

E-mail: alperbaba@iyte.edu.tr

Keywords: Stibnite, scaling, Büyük Menderes Graben

ABSTRACT

Scaling in geothermal sites is one of the factors decreasing the efficiency of geothermal resources. Metal silicates, calcium carbonate, and calcium sulfate are the most common types of scaling in geothermal fields. However, sulfides of antimony scaling are local to some geothermal areas such as Büyük Menderes Graben (BMG), where is one of the major graben systems with their geothermal capacities in Western Anatolia. The region has multi-reservoirs, and different reservoir temperatures may separate them. There are two main reservoirs in Miocene sediments; fractured and consisting of sandstone. The conglomerate is defined as the first reservoir, with a deep reservoir as the second one, represented by Menderes Metamorphic. Antimony sulfide, commonly known as stibnite (Sb_2S_3), forms in the heat-exchanger units and pipelines Büyük Menderes Graben (BMG), western Turkey. The scope of this study is to determine the source, type, and properties of the stibnite in the BMG. According to the mineral solubility diagram, stibnite starts to precipitate below ~90 °C. The result shows that the source of stibnite is *calcschists.* Also, pH and temperature change are the principal causes of stibnite deposition in the geothermal field.

1. INTRODUCTION

One of the most important graben systems of Western Anatolia, which expands in the N-S direction and has a seismically active crust, is the Büyük Menderes Graben (Dewey and Şengör 1979; Sengör 1987). The western Anatolian upper crust, which changed shape under the effect of these extensional forces, was broken by normal faults bounded by approximately E-W trending graben. The Büyük Menderes Graben is bounded by active E-W trending normal faults with a length of 150 km and a width of 10-20 km (Paton, 1992) (Fig. 1). The BMG intersects the Alaşehir Graben east of Buldan and changes from Sarayköy to the Denizli basin (Westaway, 1993). This huge structure has several discovered geothermal resources and can be considered as a geothermal basin with a continued identification of new geothermal systems (Fig. 2). Curie point temperature studies show that the depth of the heat source is 7 km in Western Anatolia, 30 km in Eastern Anatolia, and 25 km in Central Anatolia (Aydın et al., 2005). Therefore, this graben structure creates high-temperature geothermal systems by providing optimum conditions for shallow and wide heat sources in Western Anatolia. The Germencik (Aydın) geothermal field is located at the west edge of the BMG where is well known for its high-temperature geothermal resources. A crustal-scale metamorphic core complex, the Menderes Massif, dissects the approximately east-west graben to form the most prominent features of the region. The Germencik geothermal field has many altered zones with hydrothermal fluids that lead to the formation of Sb-rich deposits in the geothermal system. In particular, stibnite-based scaling is frequently observed in western BMG. With the increase of binary cycle power plants in recent years, stibnite scaling has also increased in Turkey (Zarrouk et al., 2014). Especially in Germencik, stibnite scaling was examined, and results showed that it is between 1 and 4 mm thick, has a greyish color, and its stoichiometry is close to stibnite (Sb_2S_3) (Kaypakoğlu et al., 2015).

Stibnite (Sb_2S_3), which is the main component of hydrothermal systems, is also known as antimony trisulfide. While carbonate and silica scaling has been studied for many years in geothermal power plants, stibnite scaling is little known. Antimony occurs in trisulfide, Sb^{3+}, and pentasulfide, Sb^{5+} in natural geothermal systems (Stauffer and Thompson, 1984; White, 1967). In hydrothermal systems, stibnite scaling is controlled by pH and temperature and occurs in low-temperature equipment such as heat exchangers and condensers. The concentration of antimony in the brine is less than one ppm (Brown, 2011). However, a major problem at low-temperature and pH in binary cycle power plants because antimony can still be deposited as stibnite in natural geothermal systems. Antimony is found in sulfide deposits such as stibnite, sulfosalts, and, in some cases, natural Sb, and dissolves in water in the form of hydroxide (Williams-Jones and Norman, 1997). The dissolution of stibnite in water is explained by the following equation.

$$Sb_2S_3 + 6H_2O = 2Sb(OH)_3 + 3H_2S \quad (1)$$

As can be seen from Eq. 1, as the amount of deposited stibnite increases, the amount of hydrogen sulfide also increases. Ellis and Mahon (1977) stated that stibnite could also cause corrosion in geothermal systems. Recently, studies describing and preventing this type of scaling have started to appear in the literature (Kaypakoğlu et al., 2015; Çiftçi et al., 2020).

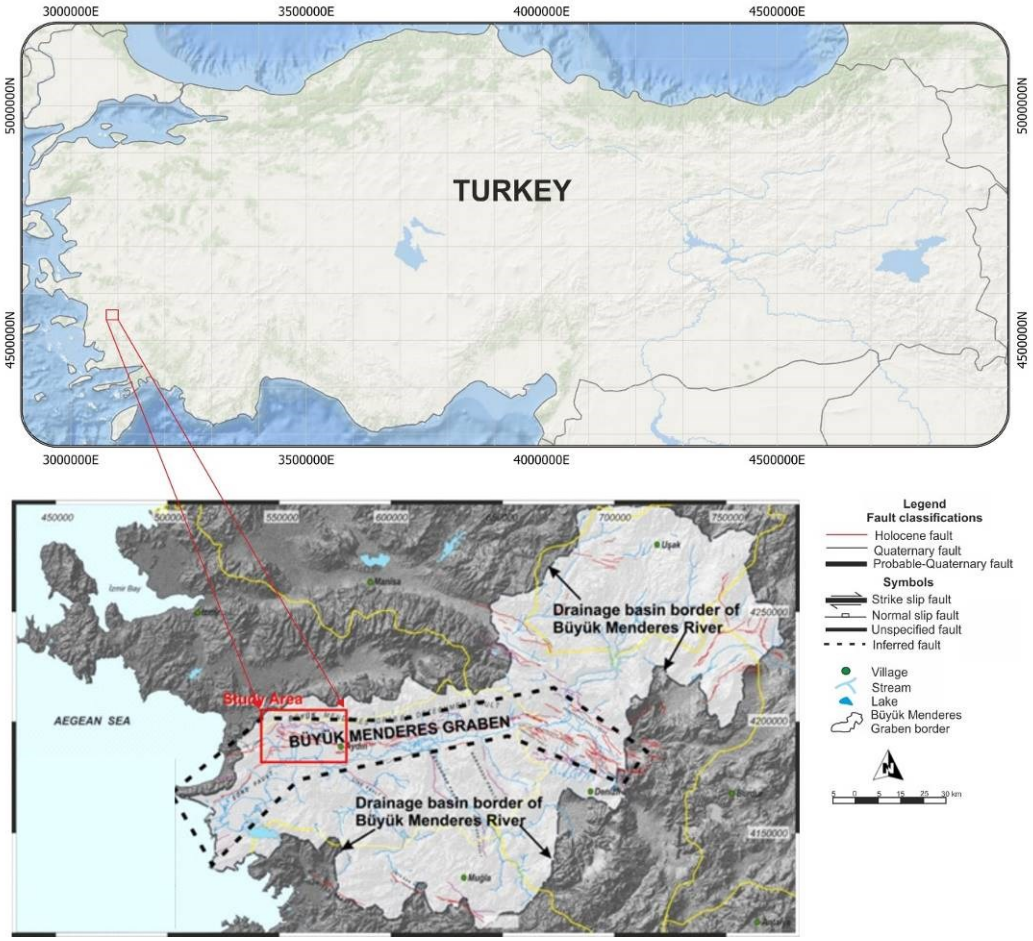

Figure 1: Location map of the study area

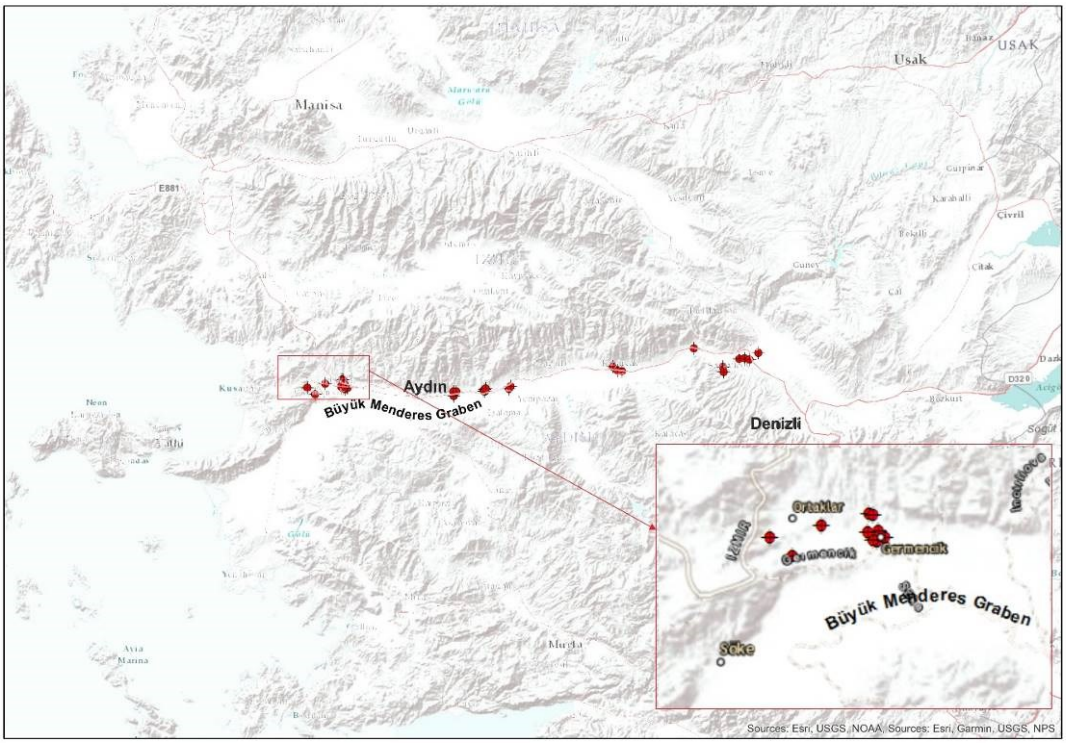

Figure 2: Geothermal power plants (red circle) around the Germencik region

2. THE SITE DESCRIPTION

The Büyük Menderes Graben is located in crystalline Menderes massif, which is the largest metamorphic massif in Turkey. This graben, which has been broken by normal faults during the alpine orogenesis, presents a dome-like structure. The Menderes Massif consists of metamorphic rocks that include schists and dolomitic marbles. Sediment deposits overlie them. Geological and geophysical studies showed stepwise graben development, which is an important characteristic of geothermal fields, occurred in the northern part of the graben (Faulds, 2010). The geological history of the Menderes Massif can be divided into paleotectonic evolution and neotectonic evolution. Magmatism, metamorphism, and deformations occurred in the paleotectonic evolution of the Menderes Massif. Rock units exposed in the vicinity of Büyük Menderes Graben can be classified into two groups: the basement and basin-fill units. Metamorphic rocks belonging to Menderes Massif constitute the pre-Neogene basement units, which is an extensional metamorphic core complex in the Western Anatolian extensional province (Bozkurt, 2001). The basin fill consists of four sedimentary packages formed on the metamorphic rocks of the Menderes Massif (Sözbilir and Emre, 1990; Bozkurt, 2000). The first sedimentary package is made up of blocky conglomerates and conglomerates containing block-sized components. With these features, the first sedimentary packages show the characteristics of an alluvial fan from west to east. The sediments belonging to the second sedimentary package are characterized by reddish colored terrestrial conglomerate and sandstone. The third sedimentary package is composed of dominant conglomerate and sandstone alternation. The facies characteristics of this unit indicate that it is controlled by E-W trending faults. The sediments of the fourth sedimentary package are formed by the alluviums that fill the Büyük Menderes Graben today. These sediments are made up of fine-grained river sediments carried by the Büyük Menderes River. The sequence continues its formation today (Sözbilir, 2001). The most important characteristic of the BMG is asymmetry, which means a steeper northern side, and most of the hot springs are concentrated along the northern side. Intersection regions between N–S Miocene grabens and the actual E–W grabens in the BMG have a suitable fractured medium for the formation of geothermal systems. Thanks to the geological formation and active tectonism, Büyük Menderes Graben has a great advantage in terms of geothermal. To illustrate, although most of these geothermal systems are located in reservoirs with medium enthalpies, which have 120−180 °C, the Germencik and Kızıldere geothermal fields are two of the hottest, largest, and have water-dominated hydrothermal reservoirs discovered in Turkey so far. The Kızıldere geothermal field has approximately 245°C reservoir temperature, whereas The Germencik field has temperatures up to 276 °C (Tureyen et al., 2016). This high temperature in the reservoir is the rapid rise of the upper crust, causing erosion and high heat flow. During the uplift period, metamorphic rocks were broken due to the effect of detachment faults, causing the geothermal fluid to rise in the region. The reservoirs of the Germencik and Kızıldere geothermal fields are located in metamorphic rocks with different lithological units. The most important feature of these metamorphic rocks is that they have a deeply located gneiss layer overlying them. The conceptual model of the study area is given in Figure 3.

The study area has two reservoirs. The first consists of mainly Neogene aged conglomerate and sandstone. The second includes Menderes Metamorphic rocks. Quartzite, quartzite-schist, calcschist, mica schist, graphite schist, gneisses are basement rocks of the geothermal system. The main fault systems in the study area are located in the north and west of the site. A detailed geology map of the study area is given in Figure 4. The geothermal reservoir rocks in the geothermal field are Neogene limestones, Paleozoic marbles, and quartzite schist in the basement complex. In addition to graben morphology formed under the extensional tectonic regimes of the region, the Menderes massif has gained its present position along the low-angle normal faults of the Oligo-Miocene period. At the same time, as a result of tectonics, a favorable environment has been formed for geothermal systems in the region.

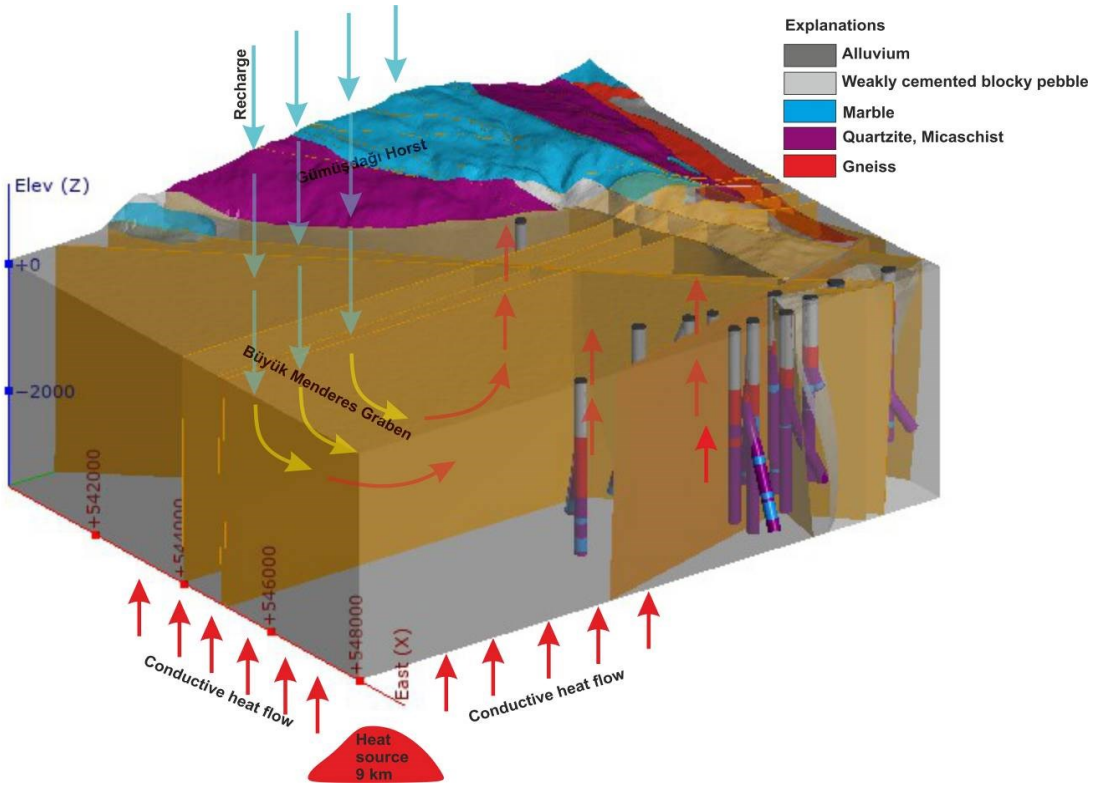

Figure 3: 3D Geothermal conceptual model of the study area

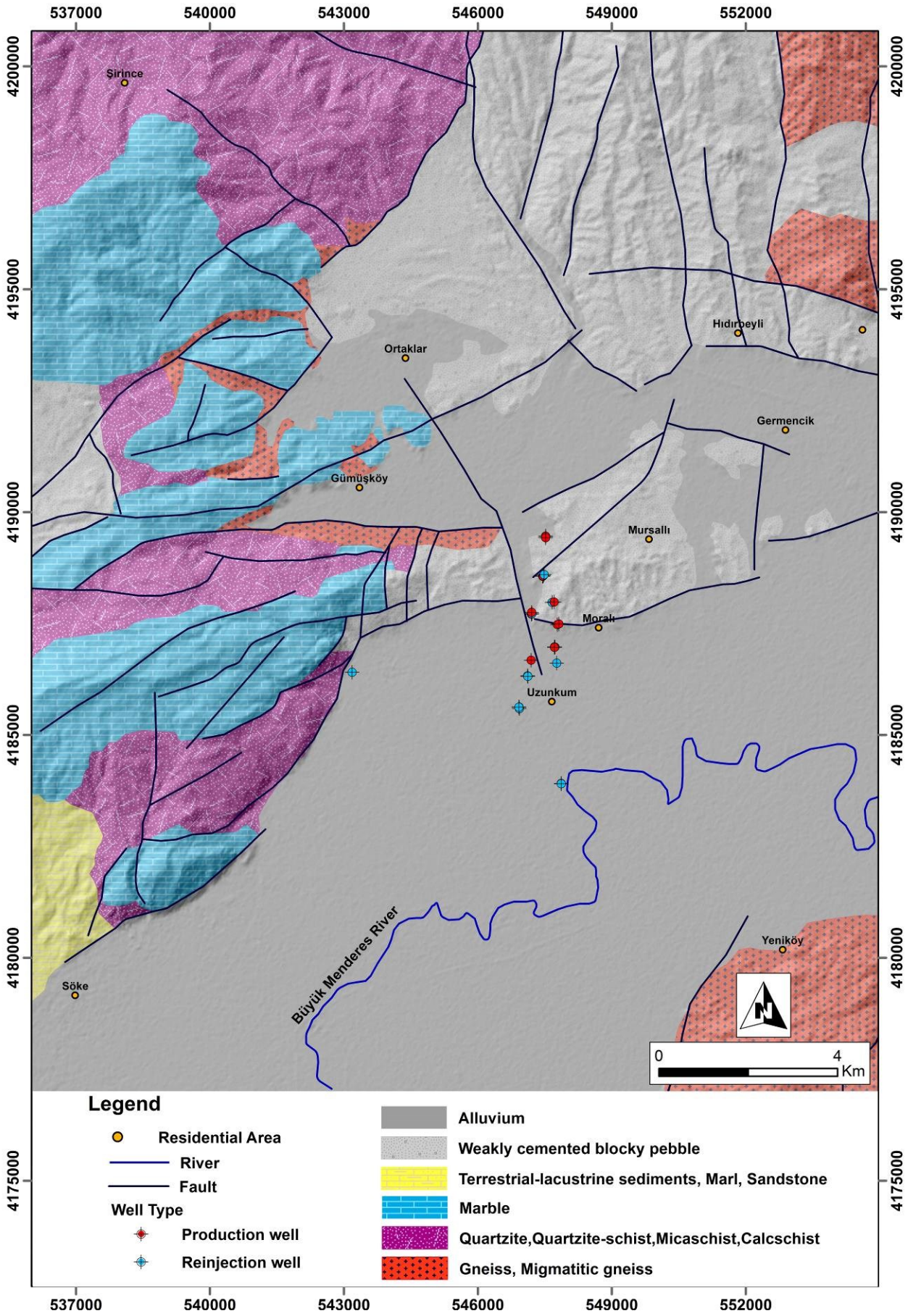

Figure 4: Geology map of the study area

3. FINDINGS

3.1 Hydrogeochemical properties of the geothermal fluid

Eleven thermal waters were sampled from the Germencik geothermal site to evaluate the chemistry of the fluid (Fig. 5). The surface temperature and the electrical conductivity (EC) of geothermal fluids range from 64.5 to 148 °C and from 5937 to 7507 µS/cm, respectively (Table 1). The highest surface temperatures are seen in the W_TR_009, W_TR_007, and W_TR_010 wells. Total dissolved solids (TDS) of the geothermal fluids range from 3700 to 4600 ppm.

The characteristics of geothermal fluids obtained from BMG changes from site to site. High-temperature wells of Gümüşköy (Aydın) are characterized by higher mineralization dominated by the ions Na^+, K^+, and Cl^-, HCO_3^-. The ionic composition of water is expressed in milliequivalents per liter (meq/l) (Fig. 6). The distribution of water types of geothermal fluids is shown in Figure 6. As can be seen from the pie diagrams, the geothermal fluid in the study area is Na-Cl-HCO_3 type. The fluid samples in the study area reflect the same water type (Table 2). There is a slight increase in Ca^{2+} values towards the north. According to the Piper triangle diagram (Fig. 7), geothermal fluids represent Na-Cl water types. The increase in Na^+, K^+, and Cl^- values in the Schoeller diagram indicates that the geothermal fluids are recharged directly from a deep reservoir (Fig. 7). This is related to water-rock interaction in the system. There is a similar relationship between geothermal fluids in the Schoeller diagram. This is because geothermal fluids are waters of the same origin and the same reservoir.

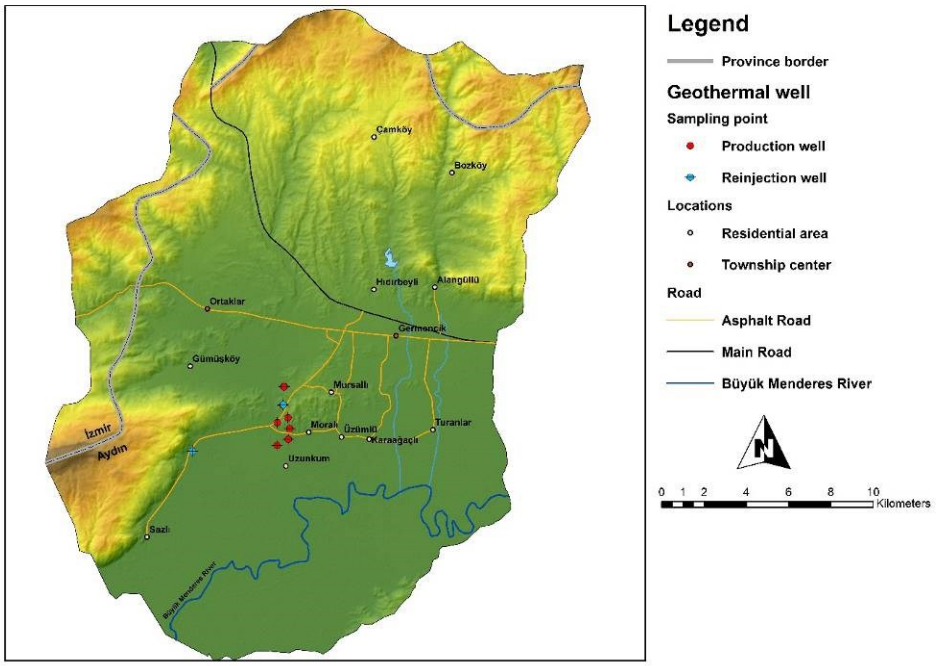

Figure 5: Sampling points in the Germencik geothermal field

Table 1: Physical properties of the geothermal fluid

No	Well ID	pH	EC µS/cm	T (°C)	TDS (ppm)	Depth (m)	Well type
1	W_TR_001	7.1	5937	125.3	3700	3328	Production
2	W_TR_002	6.87	5961	134.36	3900	3165	Production
3	W_TR_003	8.24	6030	140.06	3700	3074	Production
4	W_TR_004	8.54	6101	140.57	4000	3135	Production
5	W_TR_005	7.82	5999	138.4178	3900	3135	Production
6	W_TR_006	7.35	7507	132.13	4600	1449	Production
7	W_TR_007	8.47	6131	145.76	4100	2425	Production
8	W_TR_008	7.62	6147	64.83	3900	2907	Reinjection
9	W_TR_009	6.7	5697	148.09	3900	2568.34	Production
10	W_TR_010	6.85	6049	143.65	3800	2680	Production
11	W_TR_011	7.45	6131	64.51	4000	3525	Reinjection

Table 2: Chemical properties of the geothermal fluid

No	Well ID	Ca^{2+}	Mg^{2+}	Na^{+}	K^{+}	Cl^{-}	SO_4^{2-}	HCO_3^{-}	SiO_2	Water Type
1	W_TR_001	7.402	2.648	1324.56	64.03	1312.33	37.41	1180.21	125	Na-Cl-HCO_3
2	W_TR_002	6.898	1.752	1319.22	62.64	1305.01	34.86	1230.54	145	Na-Cl-HCO_3
3	W_TR_003	14.414	1.584	1319.41	59.97	1328.42	38.12	1148.03	140	Na-Cl-HCO_3
4	W_TR_004	8.687	1.007	1355.79	63.59	1344.67	38.68	759.72	155	Na-Cl-HCO_3
5	W_TR_005	32.533	2.379	1301.49	65.99	1308.80	34.29	1206.28	150	Na-Cl-HCO_3
6	W_TR_006	75.937	6.794	1561.63	84.93	1652.03	26.65	1710.7	145	Na-Cl-HCO_3
7	W_TR_007	13.191	0.757	1352.62	64.77	1352.37	35.5	904.77	165	Na-Cl-HCO_3
8	W_TR_008	25.084	1.884	1352.98	65.92	1340.18	31.63	1313.15	165	Na-Cl-HCO_3
9	W_TR_009	12.179	0.797	1224.32	62.44	1225.77	34.25	1153.21	165	Na-Cl-HCO_3
10	W_TR_010	44.563	3.394	1281.19	66.22	1250.75	31.22	1447.48	140	Na-Cl-HCO_3
11	W_TR_011	24.537	1.748	1345.58	66.38	1337.69	32.47	1356.18	135	Na-Cl-HCO_3

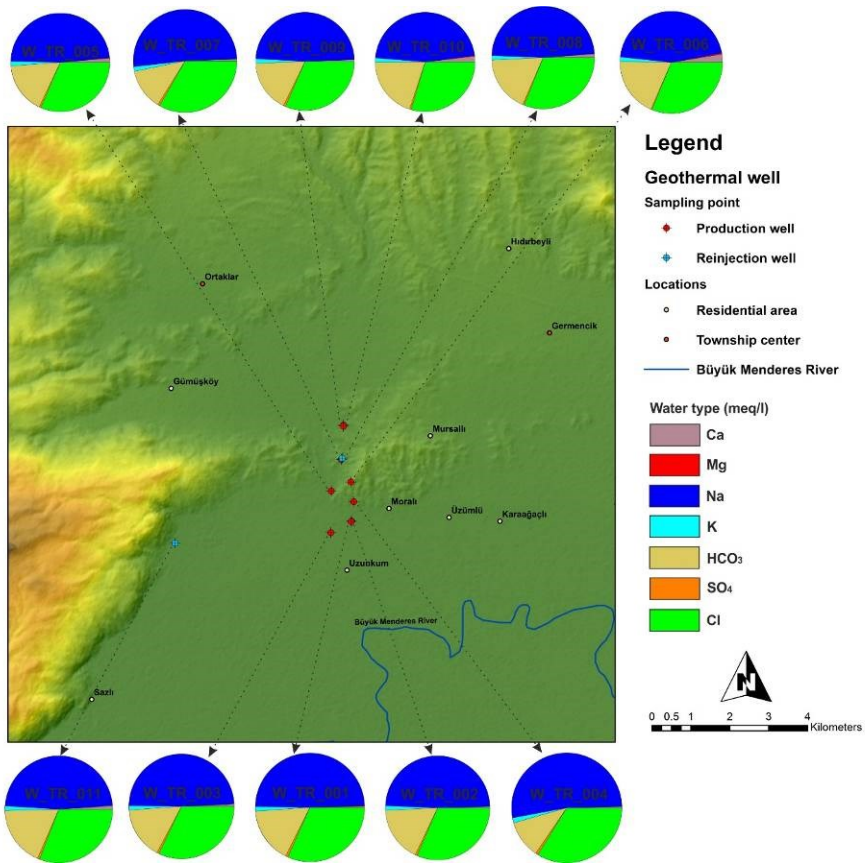

Figure 6: Demonstration of the chemical properties of the geothermal wells in the Germencik power plant

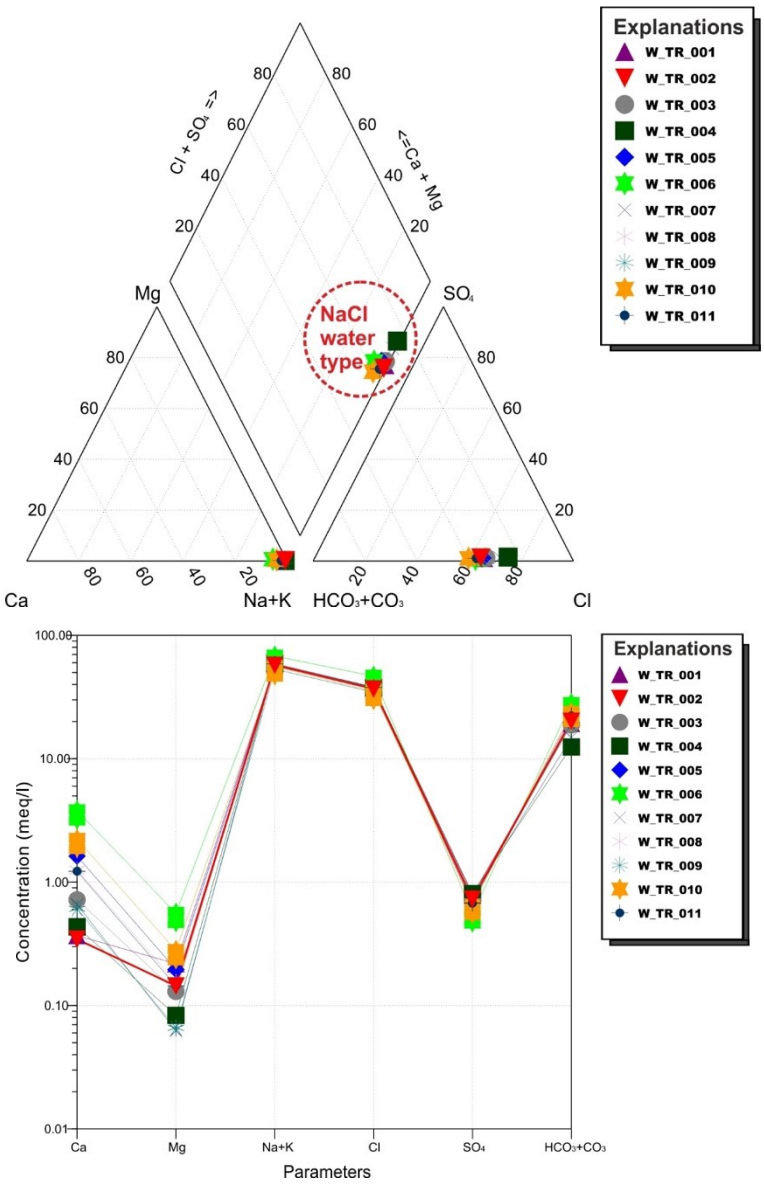

Figure 7: Piper and Schoeller diagrams of the geothermal fluid

3.2 Saturation index modeling

It is important to dispose of geothermal fluid by reinjection into shallow or deep geothermal wells. The temperature and pH changes may cause the oversaturation of some minerals, such as stibnite, thus creating a tendency to precipitate in geothermal wells. It is important to identify the state of mineral saturation in the geothermal waste fluid that will be disposed of by reinjection to find the optimum temperature for reinjection. This is possible by determining the saturation index of minerals. To evaluate this chemical content gained by the geothermal fluids, the saturation states of geothermal fluids according to various minerals were evaluated using the PHREEQC (Parkhurst and Appelo, 1999) software. The parameters used in modeling are given in Table 1 and Table 2. In saturation index diagrams, if saturation index (SI) < 0, the geothermal fluid is not saturated with the relevant mineral. SI = 0, the geothermal fluid is in equilibrium with the mineral. If SI > 0, the geothermal fluid is saturated with the relevant mineral. According to the mineral solubility diagram, stibnite precipitation should be expected in surface installations such as the heat exchanger. As can be seen from the graphs, stibnite starts to precipitate below 90°C (Fig. 8).

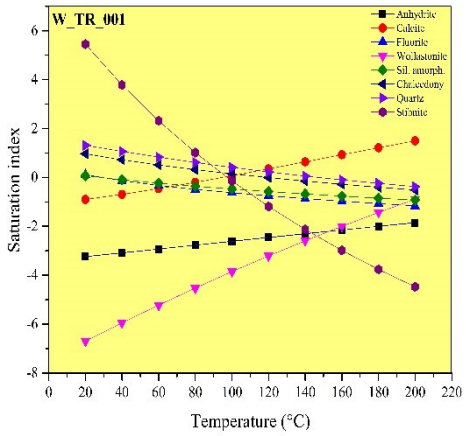
W_TR_001
Anhydrite
Calcite
Fluorite
Wollastonite
Sil. amorph.
Chalcedony
Quartz
Stibnite
Saturation index
Temperature (°C)

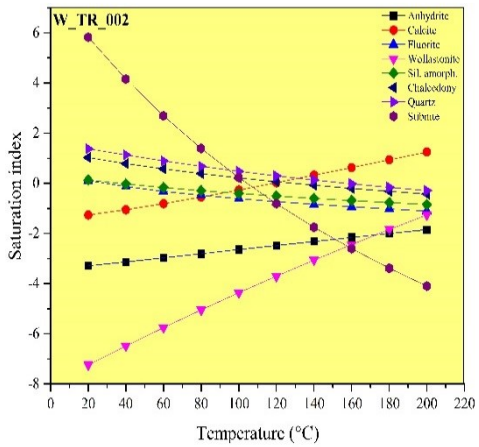
W_TR_002
Anhydrite
Calcite
Fluorite
Wollastonite
Sil. amorph.
Chalcedony
Quartz
Stibnite
Saturation index
Temperature (°C)

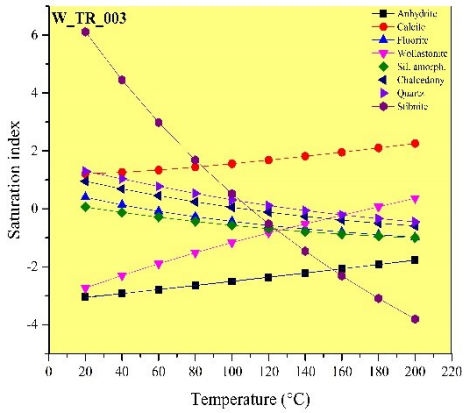
W_TR_003
Anhydrite
Calcite
Fluorite
Wollastonite
Sil. amorph.
Chalcedony
Quartz
Stibnite
Saturation index
Temperature (°C)

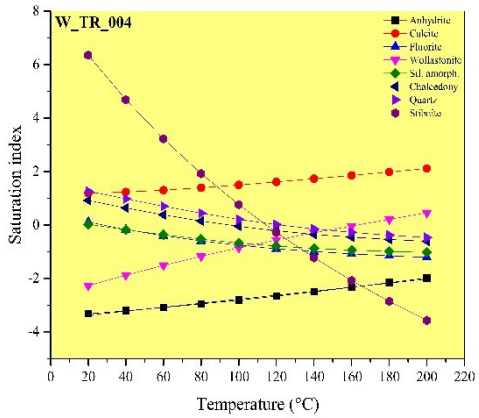
W_TR_004
Anhydrite
Calcite
Fluorite
Wollastonite
Sil. amorph.
Chalcedony
Quartz
Stibnite
Saturation index
Temperature (°C)

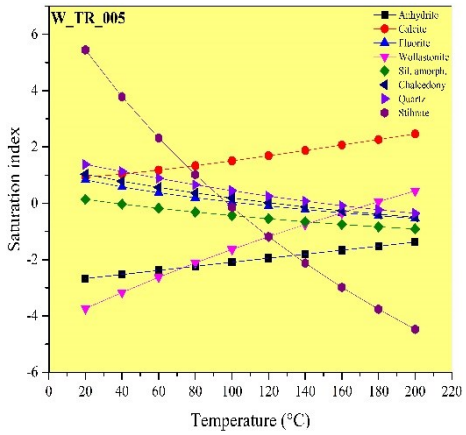
W_TR_005
Anhydrite
Calcite
Fluorite
Wollastonite
Sil. amorph.
Chalcedony
Quartz
Stibnite
Saturation index
Temperature (°C)

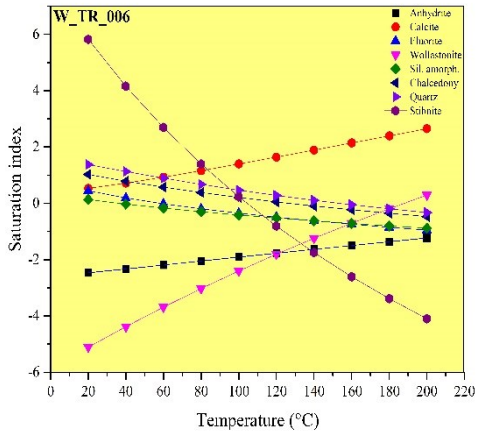
W_TR_006
Anhydrite
Calcite
Fluorite
Wollastonite
Sil. amorph.
Chalcedony
Quartz
Stibnite
Saturation index
Temperature (°C)

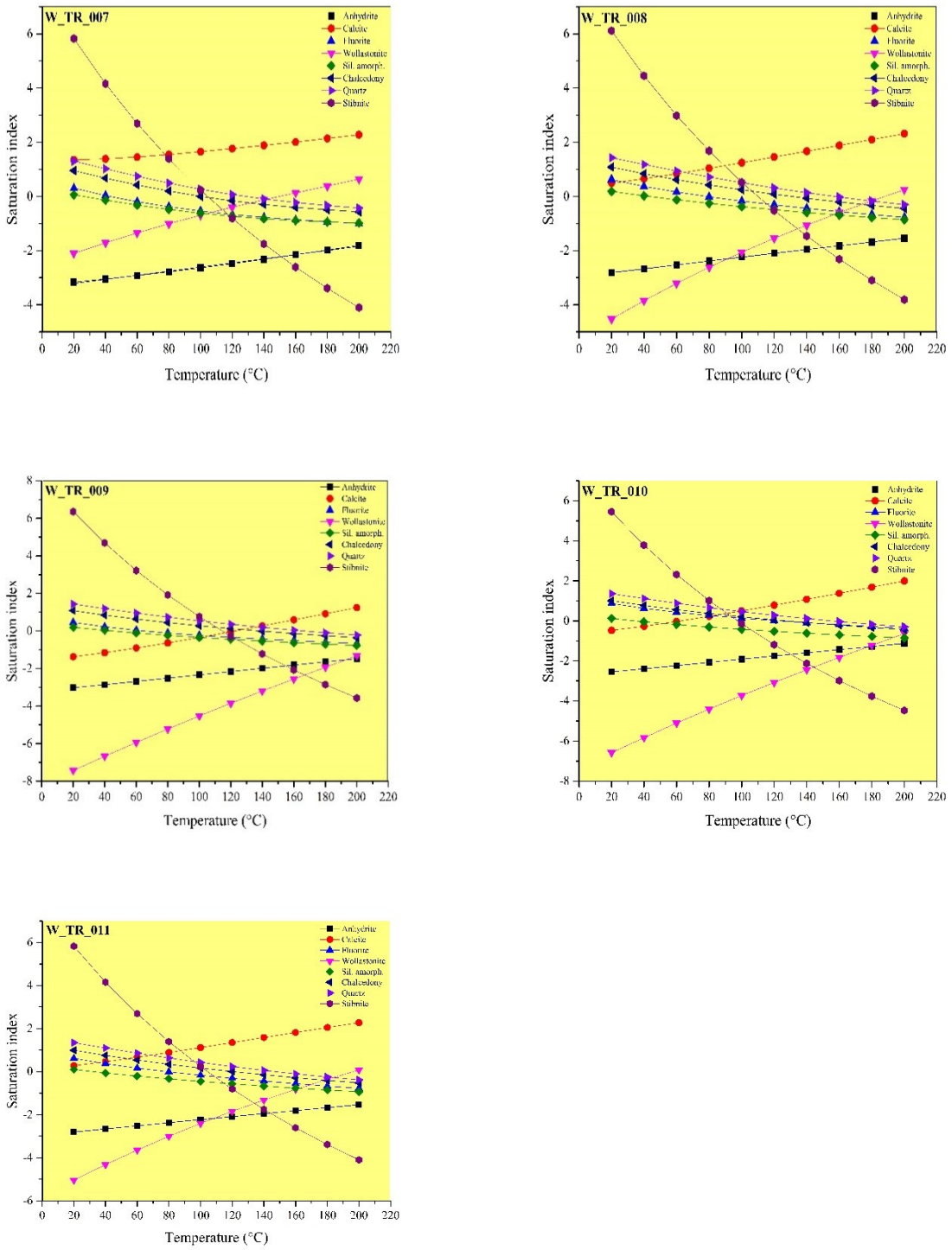

Figure 8: Saturation index graphs of the geothermal fluid

3.3 Modelling antimony species in geothermal fluid

Knowledge of the speciation and thermodynamics of minerals in a geothermal fluid is crucial to the understanding and accurate modeling of the geothermal fluid. It is known that geothermal reservoir fluids often contain small concentrations of antimony. Antimony is found in sulphide deposits as stibnite, sulfosalts, and in some cases, natural Sb (Williams-Jones and Norman, 1977). In natural geothermal systems, antimony usually occurs in two oxidation states. These are trisulphide, $Sb^{3+,}$ and pentasulphide, Sb^{5+} (White, 1967; Stauffer and Thompson, 1984).

Stibnite (Sb_2S_3), known as antimony trisulphide, is a sulphur mineral and is the main component of hydrothermal systems. In hydrothermal systems, stibnite precipitation is controlled by pH and temperature. For this reason, stibnite scaling is common in condensers, heat exchangers where the temperature and pH are low in binary cycle power plants. Although the concentration of antimony in the brine is low, antimony sulphide scaling is a major problem at low temperature and pH in binary cycle power plants. Typical antimony concentrations are less than 1 ppm in brine (Brown, 2011). However, studies have shown that antimony can be stored as stibnite in natural geothermal systems.

$$\Delta G = -RT \ln K + RT \ln Q = RT \ln \frac{Q}{K} \tag{2}$$

where Q is the ion activity product for the mineral-water reaction, K is the equilibrium constant, R is the gas constant and T is the temperature.

We have undertaken a study of the simultaneous solubilities of stibnite in brine from 50 to 200°C in the presence of 18.19 ppm H_2S in the Germencik geothermal field to provide a thermodynamically consistent. Stibnite concentrations ranged from 0.0009 to 1.23 ppm in brine. The molecular weight of H_2S is 34.1 g/mol. It has a density of 4.63 g/ml. The melting point is 550ºC. We assumed that the activity coefficient α, of H_2O is 1. The solubility of stibnite in a geothermal fluid is constant between 290 and 320°C (Zakaznova-Iakovleva et al., 2001). Therefore, it took the temperature ranges between 50 and 200°C in the geochemical model. Antimony (Sb) concentrations were evaluated to develop a predictive model for stibnite precipitation in the geothermal power plant. The aim of this was to obtain thermodynamic information on Sb (III) speciation in different temperatures in order to be able to observe the behavior of antimony in the hydrothermal system.

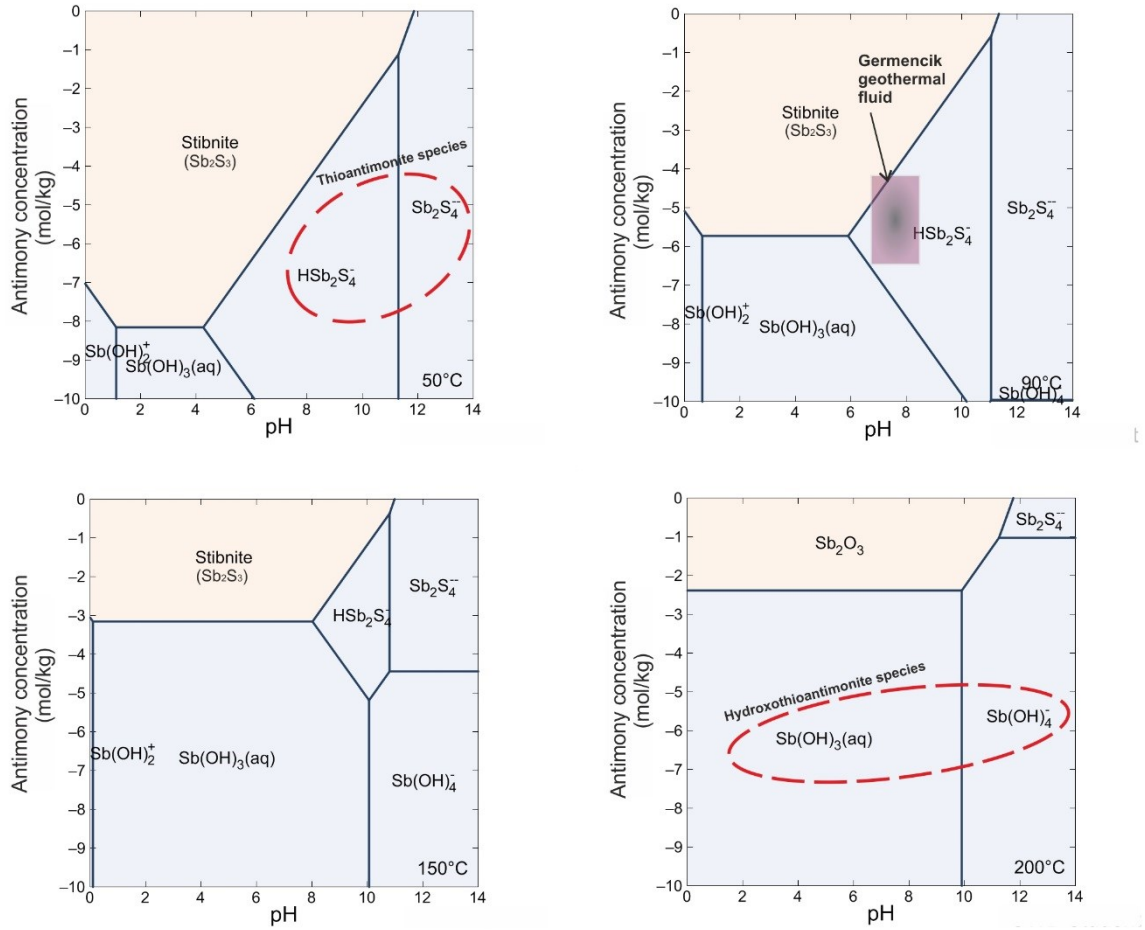

Figure 9: Stibnite species diagram in different temperature scales

At 50 and 90°C solubility of the stibnite is controlled by the thioantimonite, $HSb_2S_4^-$, $Sb_2S_4^-$. Hydroxothioantimonite species, $Sb(OH)_3$, $Sb(OH)_4^-$ become more dominant at 150 and 200°C in the geothermal fluid. As the temperature and pH, values decrease, the predominance of stibnite in the geothermal fluid increases. This means that stibnite precipitates at low temperatures and pH values. In the study area, the pH values of the geothermal fluid vary between 6.7 and 8.54 (Table 1). We know stibnite starts to

precipitate below 90°C from saturation indexes modeling in the Germencik geothermal field. As can be seen in Figure 9, at 90°C, thioantimionite species begin to dominate. Acidification occurs in the geothermal fluid due to the oxidation of hydrogen sulfide (H_2S) in this region. Acidification of the liquid causes a dramatic decrease in solubility and leads to stibnite precipitation. Therefore, in the dominant region of thioantimonite species (pink rectangle at 90°C), pH has a significant effect on stibnite solubility. Hence, low temperature and pH values should be avoided in the system, and the pH of the environment should be increased by using chemicals such as NaOH to prevent stibnite precipitation.

4. CONCLUSIONS

The study area is located in the Büyük Menderes Graben, one of the largest graben systems in Western Anatolia. The Büyük Menderes Graben has wide graben structures due to its geological feature and has led to the development of many geothermal systems. In the study area, the Menderes Metamorphic Massif containing Paleozoic aged quartz schists, mica schists, and calcschists form the reservoir rocks of the geothermal system. These units are overlain by Neogene sedimentary units with an angular unconformity. In water chemistry studies, it is seen that the pH of thermal waters varies between 6.7 and 8.54. The electrical conductivity values are between 5697 and 6147µS/cm. Thermal waters reflect Na-CI-HCO_3 water type according to Piper and Schoeller diagrams. In the study area, stibnite precipitation is the most crucial problem for affecting the efficiency of the geothermal power plant. Stibnite reduces power plant efficiency by creating scaling in low-temperature equipment, especially in binary power plants. According to the mineral saturation indexes diagram, stibnite starts to precipitate below 90°C. Therefore, considering this in the production wells, the optimum reinjection temperature is 95°C to prevent stibnite precipitation in the Germencik geothermal field. Antimony (Sb) concentrations were also evaluated to develop a predictive model for stibnite precipitation in the geothermal power plant. According to the simultaneous solubilities of stibnite in brine from 50 to 200°C, different stibnite species emerged. In the thermal water, the solubility of the stibnite is controlled by the thioantimonite species, HSb_2S_4-, $Sb_2S_4^-$ at 50 and 90°C. Hydroxothioantimonite species, $Sb(OH)_3$, $Sb(OH)_4^-$ become more dominant at 150 and 200°C in the geothermal fluid. Being the dominant region of thioantimonite species below 90°C means pH has a significant effect on stibnite solubility. In low temperatures, acidification occurs in the hydrothermal system due to the oxidation of hydrogen sulfide. Hence, low temperature and pH values should be avoided in the system, and the pH of the environment should be increased by using chemicals such as NaOH to prevent stibnite precipitation.

ACKNOWLEDGMENTS

This project encoded Reflect has received funding from the European Union's Horizon 2020 research and innovation programme under agreement No: 850626.

REFERENCES

Aydın, İ., Karat, H. İ., & Koçak, A. (2005). Curie-point depth map of Turkey. *Geophysical Journal International*, *162*(2), 633-640.

Bozkurt, E. (2000). Timing of extension on the Büyük Menderes Graben, western Turkey, and its tectonic implications. *Geological Society, London, Special Publications*, *173*(1), 385-403.

Bozkurt, E. (2001). Neotectonics of Turkey–a synthesis. *Geodinamica acta*, *14*(1-3), 3-30.

Brown, K. (2011). Antimony and arsenic sulfide scaling in geothermal binary plants. In *International Workshop on mineral scaling in geothermal environments, Philippines* (pp. 103-106).

Çiftçi, C., Karaburun, E., Tonkul, S., Baba, A., Demir, M. M., & Yeşilnacar, M. İ. (2020). Testing the Performance of Various Polymeric Antiscalants for Mitigation of Sb-Rich Precipitates Mimicking Stibnite-Based Geothermal Deposits. *Geofluids*, *2020*.

Dewey, J. F., & ŞENGÖR, A. C. (1979). Aegean and surrounding regions: complex multiplate and continuum tectonics in a convergent zone. *Geological Society of America Bulletin*, *90*(1), 84-92.

Ellis, A. J., & Mahon, W. A. J. (1977). *Chemistry and geothermanl systems* (No. 553.79 E4).

Faulds, J., Coolbaugh, M., Bouchot, V., Moek, I., & Oguz, K. (2010, April). Characterizing structural controls of geothermal reservoirs in the Great Basin, USA, and Western Turkey: developing successful exploration strategies in extended terranes.

Kaypakoglu, B., Aksoy, N., Serpen, U., & Sisman, M. (2015). Stibnite scaling in a binary power plant in Turkey. In *Proceedings*.

Parkhurst, D. L., & Appelo, C. A. J. (1999). User's guide to PHREEQC (Version 2): A computer program for speciation, batch-reaction, one-dimensional transport, and inverse geochemical calculations. *Water-resources investigations report*, *99*(4259), 312.

Paton, S. M. (1992). *The relationship between extension and volcanism in western Turkey, the Aegean Sea and central Greece* (Doctoral dissertation, University of Cambridge).

Sözbilir, H., & Emre, T. (1990, October). Neogene stratigraphy and structure of the northern rim of the Büyük Menderes graben. In *Proceedings of International Earth Science Colloquium on the Aegean Region* (Vol. 2, pp. 314-322).

Sözbilir, H. (2001). Nazilli ve dolayının (Büyük Menderes Grabeni) genç-tektoniği. *Büyük Menderes Depremleri Jeofizik Toplantısı*, 54-61.

Stauffer, R. E., & Thompson, J. M. (1984). Arsenic and antimony in geothermal waters of Yellowstone National Park, Wyoming, USA. *Geochimica et Cosmochimica Acta*, *48*(12), 2547-2561.

Şengör, A. M. C. (1987). Cross-faults and differential stretching of hanging walls in regions of low-angle normal faulting: examples from western Turkey. *Geological Society, London, Special Publications*, *28*(1), 575-589.

Tureyen, O., Gulgor, A., Erkan, B., & Satman, A. (2016). Recent expansions of power plants in Figuris concession in the Germencik geothermal field, Turkey. In *Proceedings*.

Zakaznova-Iakovleva, V. P., Migdisov, A. A., Zakaznova-Iakovlevaa, V. P., Migdisov, A. A., Suleimenov, O. M., Williams-Jones, A. E., & Alekhin, Y. V. (2001). An experimental study of stibnite solubility in gaseous hydrogen sulphide from 200 to 320 C. *Geochimica et Cosmochimica Acta*, *65*(2), 289-298.

Zarrouk, S. J., Woodhurst, B. C., & Morris, C. (2014). Silica scaling in geothermal heat exchangers and its impact on pressure drop and performance: Wairakei binary plant, New Zealand. *Geothermics*, *51*, 445-459.

Westaway, R. (1993). Neogene evolution of the Denizli region of western Turkey. *Journal of Structural Geology*, *15*(1), 37-53.

Williams-Jones, A. E., & Norman, C. (1997). Controls of mineral parageneses in the system Fe-Sb-SO. *Economic Geology*, *92*(3), 308-324.

White, D. E. (1967). Mercury and base-metal deposits with associated thermal and mineral waters. *Geochemistry of hydrothermal ore deposits*, 575-631.